

# Quantitative Analysis of the Chromatin Proteome in Disease Reveals Remodeling Principles and Identifies High Mobility Group Protein B2 as a Regulator of Hypertrophic Growth\*

Sarah Franklin<sup>‡§</sup>, Haodong Chen<sup>‡</sup>, Scherise Mitchell-Jordan<sup>‡</sup>, Shuxun Ren<sup>‡</sup>, Yibin Wang<sup>‡¶||</sup>, and Thomas M. Vondriska<sup>‡¶||</sup>\*\*

A fundamental question in biology is how genome-wide changes in gene expression are enacted in response to a finite stimulus. Recent studies have mapped changes in nucleosome localization, determined the binding preferences for individual transcription factors, and shown that the genome adopts a nonrandom structure *in vivo*. What remains unclear is how global changes in the proteins bound to DNA alter chromatin structure and gene expression. We have addressed this question in the mouse heart, a system in which global gene expression and massive phenotypic changes occur without cardiac cell division, making the mechanisms of chromatin remodeling centrally important. To determine factors controlling genomic plasticity, we used mass spectrometry to measure chromatin-associated proteins. We have characterized the abundance of 305 chromatin-associated proteins in normal cells and measured changes in 108 proteins that accompany the progression of heart disease. These studies were conducted on a high mass accuracy instrument and confirmed in multiple biological replicates, facilitating statistical analysis and allowing us to interrogate the data bioinformatically for modules of proteins involved in similar processes. Our studies reveal general principles for global shifts in chromatin accessibility: altered linker to core histone ratio; differing abundance of chromatin structural proteins; and reprogrammed histone post-translational modifications. Using small interfering RNA-mediated loss-of-function in isolated cells, we demonstrate that the non-histone chromatin structural protein HMGB2 (but not HMGB1) suppresses pathologic cell growth *in vivo* and controls a gene expression program responsible for hypertrophic cell growth. Our findings reveal the basis for alterations in chromatin structure nec-

essary for genome-wide changes in gene expression. These studies have fundamental implications for understanding how global chromatin remodeling occurs with specificity and accuracy, demonstrating that isoform-specific alterations in chromatin structural proteins can impart these features. *Molecular & Cellular Proteomics* 11: 10.1074/mcp.M111.014258, 1–12, 2012.

Transcriptional regulation must be preceded by nonrandom structural reorganization of the genome, such that stimulus-specific transcriptional regulators are recruited to the correct genomic regions and excluded from the wrong ones. During mitosis, eukaryotic chromosomes adapt an ordered and stunningly reproducible three-dimensional structure. During interphase, however, and in cells that do not divide (such as adult cardiomyocytes and neurons), the structure of the genome is much less clear. Chromosome territories have been described (1) that are thought to facilitate co-localization of similarly regulated genes within the nucleus, and recent advances in chromosomal conformation capture techniques have provided exciting new insights into the global structure of the interphase genome suggesting that the structure resembles a fractal globule (2). However, changes in this structure following stimulation, and the specific proteins responsible for dynamics of genomic structure, are less well understood.

From a structural standpoint, DNA (~146–147 base pairs) is packaged around the nucleosome octamer (3), itself composed of two copies each of four core histones (H2A, H2B, H3, and H4). Previous work has described a 30-nm fiber level feature (4), and it has been shown that chromatin structural molecules such as histone H1 (5–7) and high mobility group proteins (8, 9) contribute to higher order structure and that core nucleosome histone variants (10) may alter DNA packaging. The ability of histone-modifying enzymes to alter gene expression, presumably by altering chromatin compaction, has been well studied in various cell types and disease states (11–13). These chromatin remodelers, however, are insuffi-

From the Departments of <sup>‡</sup>Anesthesiology, <sup>¶</sup>Medicine/Cardiology, and <sup>||</sup>Physiology, David Geffen School of Medicine, University of California, Los Angeles, Los Angeles, California 90095

Received September 12, 2011, and in revised form, January 6, 2012

Published, MCP Papers in Press, January 23, 2012, DOI 10.1074/mcp.M111.014258

cient to explain global coordination of gene expression that occurs simultaneously and across distinct loci in the genome. Toward this end, several recent investigations have employed proteomic/genomic approaches to characterize large scale changes in chromatin structure in eukaryotes (14–18). Global principles for how the entire genome is structurally remodeled for gene expression changes are lacking. We reasoned that modulation of the abundance and stoichiometry of the chromatin backbone itself could be a mechanism by which the cell rapidly alters gene expression across the genome in a coordinated manner. To test this hypothesis and address the general paucity of knowledge about chromatin-bound proteins in the heart, we have carried out a fundamentally new type of analysis of chromatin remodeling, one that quantifies the constituents of the genome protein backbone at different stages of global transcriptional activation. Our mass spectrometry data reveal the itineraries of chromatin modifiers and chromatin structural proteins during the development of disease and provide a novel blueprint for chromatin-associated proteins in the heart.

#### EXPERIMENTAL PROCEDURES

**Mouse Model of Cardiac Hypertrophy and Failure**—Adult male BALB/c mice aged 8–12 weeks (Charles River Laboratories) were used for this study. All of the protocols involving animals conform to the National Institutes of Health Guide for the Care and Use of Laboratory Animals and were approved by the UCLA Animal Research Committee. The murine model of transverse aortic banding-induced cardiac hypertrophy was performed as described previously (19–21). Animals were anesthetized with 1.5–2.0% isoflurane, intubated, and ventilated with 1.5–2.0% isoflurane in 95% O<sub>2</sub>, 5% CO<sub>2</sub>. After shaving the hair from the animal, the chest was entered from the left side via the third intercostal space; the aorta was identified at the T8 region; and a venous vascular clamp (Fine Science Tools), outfitted with a band of silastic tubing at the distal edge of one of the clamps, was placed around the vessel. The internal diameter of the resulting modified clamp was that of a 27.5-gauge needle, a common diameter for aortic banding in the mouse; the clamp is of a size that does not impede pulmonary function. Once the aorta was clamped, distal blood flow was measured and quantified using a flow probe (Transonic Instruments). The chest was then closed using 6–0 prolene suture, during which negative pressure in the thorax was reestablished by removing air with a PE-50 chest tube attached to a syringe. SHAM operated mice underwent the same procedure without placement of aortic clamp.

**Echocardiography**—ECHO was used to determine cardiac parameters in live mice as described (20, 21), including the following indices: left ventricular size (end diastolic and end systolic dimension), wall thickness (intraventricular septum and posterior wall thickness), ventricular mass, ventricular function (ejection fraction), and blood flow. ECHO was performed on mice sedated with isoflurane vaporized (2.5% for induction, 1.0% for maintenance) in oxygen. The animal's chest was shaved and positioned in the left lateral decubitus position for ultrasonic imaging with a Vevo 770 high resolution ECHO system equipped with a 35 MHz transducer. The short axis view (M-mode) and the long axis view (Doppler) measurements were performed, and data were stored for off-line analysis. LV chamber dimensions, VST, PWT, and LV mass index (the ratio of LV mass to body weight) were obtained from M-mode images; LV systolic function is also assessed from these measurements by calculating EF. All of the mice under-

went ECHO analyses once before TAC or SHAM surgery, once a day after and then once every 5 days for the duration of the study. The animals were considered “hypertrophic” when their LV mass was greater than the mean of the control animal with no depression of LV function as measured by EF; animals were considered in “failure” when the EF was significantly decreased below the mean of the control animal. These phenotypes corresponded to roughly 2 and 4 weeks after TAC surgery in most animals. Data from mice appear in Figs. 1–3 and supplemental Figs. 1–4 and 6.

**Nuclear Isolation and Fractionation**—All of the buffers used for cell isolation or fractionation in this study contained the following protease, phosphatase, and deacetylase inhibitors, respectively: 0.1 mM phenylmethanesulfonyl fluoride, protease inhibitor mixture pellet (Roche Applied Science), 0.2 mM sodium orthovanadate, 0.1 mM sodium fluoride, and 10 mM sodium butyrate.

Cardiac nuclei were isolated as previously described (22). Briefly, hearts were excised, washed in PBS, minced with scissors, and processed in a glass Dounce homogenizer in buffer containing 10 mM Tris (pH 7.4), 250 mM sucrose, 1 mM EDTA, 0.15% Nonidet P-40. After homogenization the suspension was passed through a 100- $\mu$ m nylon strainer (BD Falcon, number 352360) to remove any large insoluble material. Subcellular fractionation was carried out by centrifuging at 1,000  $\times g$  to pellet crude nuclear fraction. The crude nuclear pellet was resuspended in homogenization buffer, layered on a 2 M sucrose pad, and centrifuged at 7,500  $\times g$  for 5 min to isolate the enriched nuclear fraction. All of the steps were carried out at 4 °C. The initial relative purity of the nuclei fraction was evaluated via Western blotting for compartment specific proteins and compared with unfractionated cells from the heart (whole heart lysate) using antibodies to histone H3 and GAPDH. Whole heart lysate (whole heart lysate) was made by homogenizing the entire heart in 20 mM Tris (pH 7.4), 150 mM NaCl, 1 mM EDTA, 1 mM EGTA, 1% Triton X-100, 2.5 mM sodium pyrophosphate, 1 mM  $\beta$ -glycerophosphate, followed by sonication and centrifugation at 13,000 rpm to remove insoluble material. We consistently achieve  $\geq 80\%$  enrichment of nuclei with this method as observed by electron microscopy and Western blotting analysis (22).

**Purification of Cardiac Chromatin and Nucleoplasm and Acid Extraction of Nuclear Proteins**—Following isolation of nuclei, further fractionation was carried out to separate nucleoplasm from chromatin as previously described (22). Briefly, isolated nuclei were resuspended in buffer (20 mM HEPES, pH 7.6, 7.5 mM MgCl<sub>2</sub>, 30 mM NaCl, 1 M urea, 1% Nonidet P-40) to solubilize the nuclear membrane and extract soluble proteins in the nucleoplasm. After solubilization, the samples were centrifuged at 13,000  $\times g$  for 10 min to pellet the insoluble chromatin and remove the nucleoplasm fraction. The chromatin pellet was washed with PBS; solubilized in 50 mM Tris (pH 8), 10 mM EDTA, 1% SDS; sonicated to shear the DNA; and centrifuged at 13,000  $\times g$  to extract proteins (referred to as chromatin fraction). For acid extraction, isolated chromatin was treated with 400  $\mu$ l of 0.4 N H<sub>2</sub>SO<sub>4</sub> and placed on a rotator at 4 °C overnight. The samples were centrifuged at 16,000  $\times g$  to pellet acid-insoluble material. The supernatant was treated with 132  $\mu$ l of TCA in a dropwise manner, inverting the tube between drops, and placed on ice for 30 min to precipitate the acid-extracted proteins. Precipitated proteins were collected by centrifuging at 16,000  $\times g$  for 15 min (4 °C). The pellet was washed twice with ice-cold acetone without disturbing the pellet and allowed to air dry. The pellet was resuspended in buffer containing 1% SDS, 50 mM Tris (pH 8), and 10 mM EDTA. Proteins extracted in this manner were examined in Figs. 1–3 and supplemental Figs. 2–4 and 6.

**Isolated Myocytes**—Neonatal rat ventricular myocytes (NRVMs; used in Fig. 4 and for the microarray studies in Fig. 5 and supple-

mental Fig. 5)<sup>1</sup> were obtained by enzymatic dissociation from 1-day-old litters and plated in Dulbecco's modified Eagle's medium (Invitrogen, number 11965) containing 1% penicillin, 1% streptomycin, 1% insulin-transferrin-sodium selenite supplement, and 10% fetal bovine serum for the first 24 h, after which the cells are cultured in serum- and antibiotic-free media. NRVMs were treated with 50 nM small interfering RNA targeted to HMGB1 (25 nM each SI03034696 and SI03111626; Qiagen) or HMGB2 (25 nM each SI02877252 and SI02877266; Qiagen) for 72 h. Control cells were treated with 50 nM scrambled small interfering RNA (catalog number 1027280; Qiagen). Transfections were performed with Lipofectamine RNAiMax transfection reagent (Invitrogen). For cell size analysis NRVMs were fixed with 4% paraformaldehyde, incubated with rhodamine-conjugated phalloidin (Invitrogen) to stain the actin filaments, and imaged on a Nikon Eclipse TE2000-U. The average size of treated and untreated NRVMs was quantified by measuring the area of actin staining in Photoshop (Adobe). For each condition at least 50 cells were quantified in three separate experiments. To induce hypertrophy in isolated NRVMs, the cells were treated with one of the following three hypertrophic agonists: isoproterenol (1  $\mu$ M), phenylephrine (10  $\mu$ M), or endothelin-1 (1 nM) for 48 h.

**Electrophoresis and Western Blotting**—The proteins were separated by standard SDS-PAGE using Laemmli buffer. The gels (12%) were stained with Oriole (Bio-Rad). For Western blotting, the proteins were transferred to nitrocellulose, membranes were blocked with milk, and protein signals were detected by enzyme-linked chemiluminescence (GE Biosciences). Ponceau staining of membranes was used to confirm transfer and protein loading. Antibodies used in this study were as follows, including sources: histone H3 (Abcam, ab1791, 1:10,000 dilution); histone H4 (Abcam, ab10158, 1:1000 dilution); SNRP70 (Abcam, ab51266, 1:400 dilution); HMGB1 (Abcam, ab18256, 1:1000 dilution); HMGB2 (Abcam, ab67282, 1:1000 dilution); GAPDH (Santa Cruz, sc-20357, 1:1000 dilution); histone H3-trimethylated-K9 (Abcam, ab8898, 1:500 dilution); histone H3-mono/di/tri-methylated-K4 (Millipore, 04-791, 1:1000 dilution); histone H1.0 (Abcam, ab11079, 1:1000 dilution); histone H3-trimethylated-K4 (Abcam, ab71998, 1:500 dilution); Ruvb-like 1 (Proteintech, 10210-2-AP, 1:1000 dilution). Nuclear lysate control was made by solubilizing intact nuclei in buffer containing 1% SDS, 50 mM Tris (pH 8), and 10 mM EDTA followed by centrifugation at 13,000 rpm for 15 min to remove insoluble material. HeLa lysate control was made by solubilizing HeLa cells, isolated by scraping cells from culture dishes, in 20 mM Tris (pH 7.4), 150 mM NaCl, 1 mM EDTA, 1 mM EGTA, 1% Triton X-100, 2.5 mM sodium pyrophosphate, 1 mM  $\beta$ -glycerophosphate. The homogenate was then sonicated three times for 5 s each followed by centrifugation at 13,000 rpm to remove insoluble material.

**Enzyme Digestion**—Proteins isolated from acid extraction of chromatin were separated by SDS-PAGE. Each gel lane was cut into 25 slices (~2 mm each, labeled A–Y in supplemental Fig. 2) for protein identification by mass spectrometry. Gel plugs were dehydrated in acetonitrile and dried in a SpeedVac. The samples were reduced and alkylated with 10 mM dithiothreitol and 10 mM TCEP solution in 50 mM  $\text{NH}_4\text{HCO}_3$  (30 min at 56 °C) and 100 mM iodoacetamide (45 min in dark), respectively. The gels were washed with 50 mM  $\text{NH}_4\text{HCO}_3$ , dehydrated with acetonitrile, and dried down in a SpeedVac. The gel pieces were then swollen in digestion buffer containing 50 mM  $\text{NH}_4\text{HCO}_3$  and 20.0 ng/ $\mu$ l of trypsin (37 °C, overnight). The peptides were extracted with 0.1% TFA in 50% acetonitrile solution, dried down, and resuspended in 0.1% formic acid. For each condition (basal, hypertrophy, and failure) three biological (*de novo* preparation of samples from different animals) and two technical (multiple LC-

MS/MS experiments on the same preparation) replicates were analyzed by mass spectrometry.

**Mass Spectrometry Analyses and Database Searching via SEQUEST**—Extracted peptides were analyzed by nano-flow LC-MS/MS on a Thermo Orbitrap with a dedicated Eksigent nanopump using a reversed phase column (75- $\mu$ m inner diameter 10-cm, BioBasic C18 5- $\mu$ m particle size; New Objective) and a flow rate of 200 nL/min. For peptide separation, a linear gradient was utilized from 95% Buffer A (0.1% formic acid, 2% acetonitrile) and 5% Buffer B (0.1% formic acid, 20% water in acetonitrile) to 50% Buffer A and 50% Buffer B over 60 min. The spectra were acquired in data-dependent mode with dynamic exclusion where the instrument selects the top six most abundant ions in the parent spectra for fragmentation. The data were searched against the mouse International Protein Index database (version 3.76; 57, 605 entries) using the SEQUEST algorithm (23) in the BioWorks software program version 3.3.1 SP1. The false discovery rate, which was calculated on several independent data sets within this study by reverse database searching, ranged from 1.4 to 1.7%. All of the spectra used for identification had  $\Delta\text{CN} > 0.1$ , consensus score  $\geq 20$  and met the following Xcorr criteria:  $> 3$  (+2),  $> 4$  (+3), and  $> 5$  (+4). Peptides with +1 charge were not used for identification of proteins; however, some +1 peptides were included in quantitative measurements (following manual inspection) only in the case of histone variants (see Fig. 2 and supplemental Table 7). Searches required full tryptic cleavage,  $\leq 3$  missed cleavages and were performed with the differential modifications of carbamidomethylation on cysteine and methionine oxidation. Mass tolerance was 2 Da for precursor and 1 Da for product ions. All of the proteins were identified on the basis of two or more unique peptides.

**Bioinformatics and Protein Annotation**—The molecular weight, pI, and the grand average of hydropathy score were calculated by ProtParam tool provided in the SeqUtils package of Biopython (v1.50; supplemental Fig. 3F). Protein expression plots were generated as described (24). Redundancy in proteins was eliminated at the primary sequence level by manual inspection using CLUSTAL to compare the sequences in UniProt. Genome analysis (*i.e.* for determining from where in the genome mRNAs for the detected proteins were transcribed) was performed from the NCBI genome browser following conversion of International Protein Index to ref-seq accession numbers (supplemental Figs. 3E and 4D). Gene Ontology annotation enrichment analysis was performed using the DAVID Bioinformatics Resource (v6.7) developed by the NIAID, National Institutes of Health (Figs. 3B and 5A and supplemental Fig. 4A) (25). The Interpro and Kyoto Encyclopedia of Genes and Genomes analysis functions of DAVID were utilized to determine enrichment in protein domains and functional pathways (supplemental Figs. 4, B and C, and 5, A and B).

Mass spectrometry raw data were searched two ways in this study: by "conventional" SEQUEST searching (which generated comprehensive protein lists, reported in supplemental Tables 1 and 2, and which were used to generate Fig. 2 and supplemental Table 7) and via a quantitative analysis using the Rosetta Elucidator software (from Microsoft, which led to Figs. 1 and 3 and supplemental Figs. 3, A–D, and 4D) (26, 27). The reason for this approach was that a main component of chromatin—histones—are small molecular weight proteins that yield few peptides following enzymatic digestion and that often differ by only a few amino acids. To accurately quantify them, we sought to confirm all peptide identifications manually, which is more easily done after conventional SEQUEST search. For Elucidator analyses, peptides across the entire chromatographic run for each sample were aligned between mass spectrometry runs and between conditions (basal, hypertrophy, and failure). The peak intensity for each eluting peptide was calculated as the area under the curve. To determine protein abundance, intensity data for all peptides mapping to a protein were combined, and data from three biological and two

<sup>1</sup> The abbreviations used are: NRVM, neonatal rat ventricular myocyte; GAPDH, glyceraldehyde-3-phosphate dehydrogenase.

technical replicates was averaged for each of the three conditions. Proteins whose intensity changed  $\geq 2$ -fold between conditions with a  $p$  value  $\leq 0.01$  were considered to be statistically significant. To identify modules of proteins with similar expression behavior (Fig. 3), intensity values were converted to z-scores. Proteins were then clustered using a self-organizing map with  $x$  and  $y$  nodes of 3,3 and cosine correlation. Intensity data were coupled to peptide identification, which was determined using the SEQUEST algorithm using the same criteria described above. Mass tolerance was 0.5 Da for precursor and 1 Da for product ions, and all identifications were based on at least two peptides.

**Quantitative Real Time PCR Analysis**—Total RNA was isolated from the left ventricle of the heart (supplemental Fig. 1C) or from cultured NRVMs (Fig. 4C) using TRIzol (Invitrogen) according to the manufacturer's protocol. Total RNA was transcribed using SuperScript first strand synthesis system for RT-PCR (Invitrogen) according to the manufacturer's protocol to produce cDNA. cDNA transcripts were amplified on the iCycler iQ real time PCR detection system with iQ SYBR Green Supermix (Bio-Rad). Expression levels were analyzed using the iQ5 Optical Systems software v2.0 and normalized against GAPDH by subtracting the mean cycle number for each experimental group from the mean cycle number for GAPDH from the same group. The normalized means were then applied to the formula  $(2^{-(\text{cycle}\#)})^{-1}$  to calculate fold change. Primers used in this study are as follows: GAPDH, forward 5'-CCCACTAACATCAAATGGGG-3' and reverse 5'-CCTTCCACAATGCCAAAGTT-3'; HMGB2, forward 5'-AAGCCGCGGGCAAGATGTC-3' and reverse 5'-TGCCCTTGGCACGGTATGCA-3'; ANF, forward 5'-CTGATGGATTCAAGAACCTGCT-3' and reverse 5'-CTCTGGGCTCCAATCCTGTC-3'; SERCA2a, forward 5'-CCTTC-TACCAGCTGAGTCATTT-3' and reverse 5'-CAGATGGAGCCCACG-ACCA-3';  $\alpha$ -MHC, forward 5'-GAACAGCTGGGAGAAGGGGG-3' and reverse 5'-GCCTCTGAGGCTATTCTATTGG-3'; and  $\beta$ -MHC, forward 5'-CTCAACTGGGAAGAGCATCCA-3' and reverse 5'-CCTTC-AGCAAACCTGGAGGC-3'.

**Microarrays**—Total RNA was isolated from cultured NRVMs after treatment with HMGB2 or scrambled small interfering RNA using TRIzol (Invitrogen) according to the manufacturer's protocol (Figs. 4D and 5A and supplemental Table 6). RNA was analyzed for genome-wide expression analysis using an Illumina rat bead chip (RatRef-12\_V1\_0\_R2\_11222119\_A). The RatRef BeadChip contains 22,523 probes that map to 21,791 genes in the rat genome. 200 ng of each sample was processed using the Illumina specific version of the Ambion TotalPrep 96 kit (catalog number 4393543). 750 ng of biotinylated cRNA product was added to each array hybridized according to standard Illumina protocols. Washing and signal development were performed with the aid of a SciGene model 650c microarray processor (LittleDipper). Chips were scanned on an Illumina iScan confocal scanner under standard parameters. The samples were analyzed in triplicate for each treatment group, and data for each gene were averaged between the three samples. The data were subjected to background subtraction and quantile normalization. For data analyses and figure generation, the coordinates of each probe on the microarray was extracted from the annotation file provided by Illumina. The rat genome (Baylor 3.4/m4) was used to generate Fig. 4D, with each chromosome divided into bins of 1 megabase. Only transcripts meeting a  $p$  value cutoff of 0.001 were examined and are reported.

## RESULTS

**Mass Spectrometric Measurements of the Chromatin Proteome**—To investigate changes in chromatin-bound proteins commensurate with global changes in gene expression, adult mice were subjected to cardiac pressure overload by transverse aortic constriction (19), a model that recapitulates the

human disease of heart failure (supplemental Fig. 1), which affects millions of people worldwide (28). This disease is associated with a global shift in gene expression (supplemental Fig. 1C (29)), which drives a progressive increase in cardiac mass at the cell and organ level accompanied by deterioration of cardiac function (supplemental Fig. 1B). Hearts from mice in stages of cardiac hypertrophy, failure, or basal state were excised. Chromatin was fractionated (Fig. 1A and supplemental Fig. 2) from mouse cardiac nuclei, and DNA-bound proteins were acid-extracted. As with any fractionation study of a complex tissue like the heart, complete purification of individual fractions is not possible when using a nonbiased technique like mass spectrometry for detection. Our previous work demonstrates that this method significantly enriches for histone and other chromatin-bound proteins (22), although additional studies will be required to determine what role each individual proteins have in the chromatin fraction (*i.e.* to discriminate between true residents and contaminants). Proteins were separated by SDS-PAGE, in-gel trypsin-digested, and analyzed by quantitative mass spectrometry on an Orbi-trap instrument, and peptide spectra were examined by a combination of traditional database searching (SEQUEST), label-free quantitative analysis using the Elucidator software package (26, 27), and manual inspection (please see "Experimental Procedures" and supplemental Fig. 3).

This study includes the analysis of three biological replicates (*i.e.* three different animals), two technical replicates each, in the basal, hypertrophy (moderate disease), and failing heart (severe disease) conditions, resulting in the acquisition of  $\sim 5.14$  million spectra from 450 LC-MS/MS runs. Aligning the multiple features of retention time, parent ion intensity, and MS/MS-confirmed sequence, this quantitative analysis allows for trends of protein abundance to be extracted from highly reproducible LC-MS/MS runs. Using this approach, combined with manual validation, we measured the association of  $>300$  proteins with chromatin during distinct stages of heart failure in the mouse (supplemental Tables 1–4; note that only proteins detected by mass spectrometry are reported in this study). All of the peptides used for identification are listed in supplemental Table 8. The examples of histone 1.0 and histone 1.4 represent a protein with altered abundance during the development of disease contrasted with one whose abundance is stable, respectively (Fig. 1B). Progression of disease was associated with global shifts in the abundance of chromatin-associated proteins (Fig. 1, C and D). Principle component analysis of all peptide intensities from all 18 data sets after analysis of variance indicates good separation between the three experimental groups (and good agreement within them) (Fig. 1E), supports the quantitative analysis of protein abundance, and demonstrates strong reproducibility of the experimental workflow. Genes for proteins undergoing altered expression localize without bias throughout the genome (supplemental Fig. 3), suggesting genome-wide rearrangements are a prerequisite for disease. Furthermore, annotation of

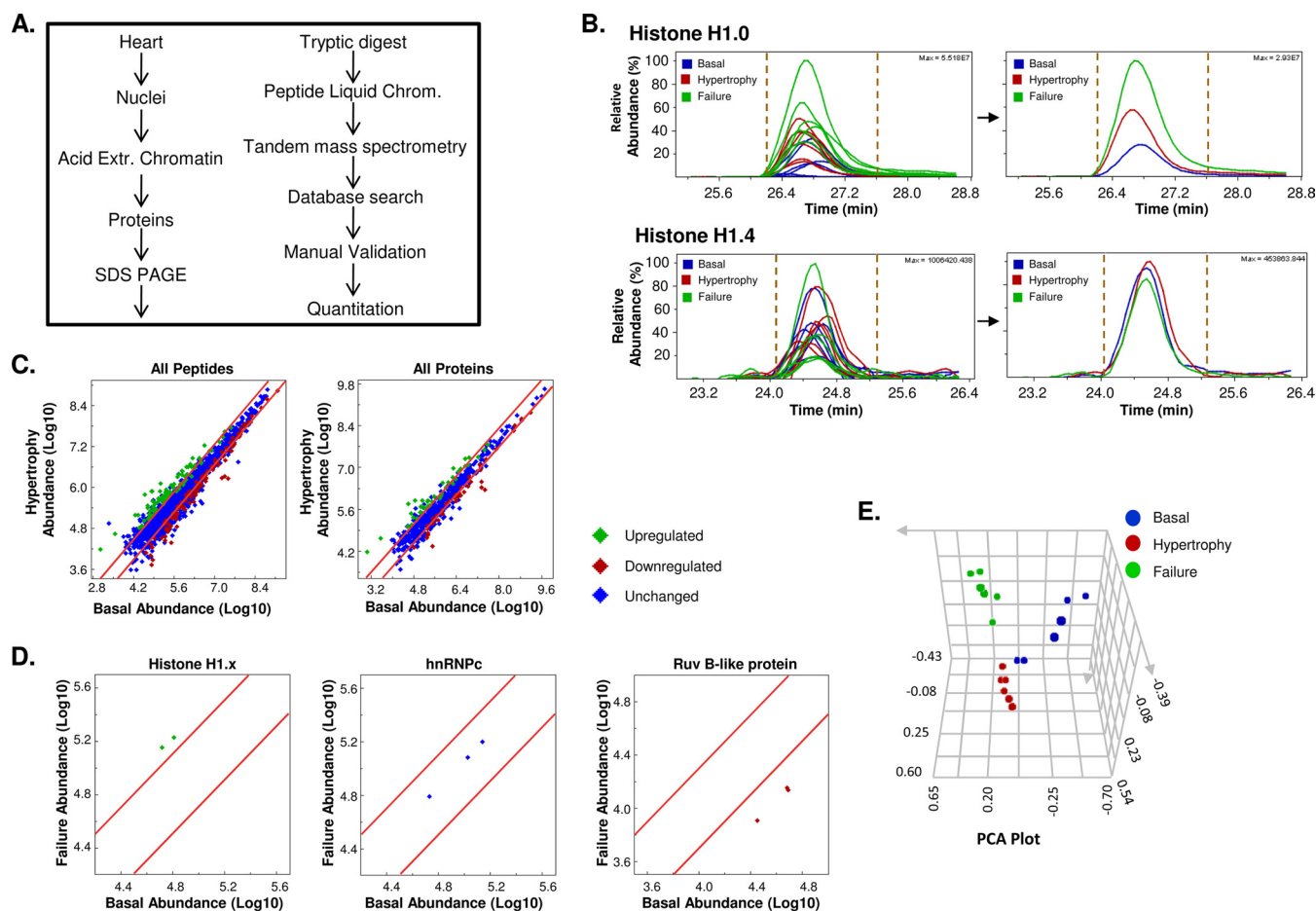


**FIG. 1. Proteomic measurement of chromatin-bound proteins.** *A*, chromatin-associated proteins were isolated by acid extraction from mouse cardiac nuclei. The proteins were electrophoretically separated, digested, and analyzed by semi-quantitative label-free mass spectrometry. All of the procedures are described in greater detail under “Experimental Procedures.” *B*, individual peptide peaks were quantified and linked with sequence information by database searching; shown are examples of histone H1.0 (*top panels*; peptide YSDM(147.0355)IVAAIQAEK), which was altered with disease compared with histone H1.4 (*bottom panels*; peptide TSGPPVSELITK), which was unchanged (see [supplemental Fig. 3](#) for expanded version of this data). In the *left panels*, the monoisotopic peptide peak from each biological and technical replicate was aligned and quantified as the area under the curve. *Dotted gold lines* indicate the area of integration used for intensity calculations. Intensity data from all six replicates were averaged for each condition (*right panels, top and bottom*). All of the peaks in the isotopic window were used for intensity calculations (see [supplemental Fig. 3, A and B](#)). Note the reproducibility in alignment and quantitation between runs. *C*, pair-wise analyses between basal and hypertrophy reveals remodeling of the chromatin protein backbone during disease (see [supplemental Tables 1–4](#) for complete details and protein identity of chromatin changes during disease, including relative quantitation data; [supplemental Fig. 3C](#) shows comparison of proteins and peptides among healthy and early and late stage disease samples). The *red lines* indicate 2-fold change; similar trends exist at the peptide (*left panel*) and protein (*right panel*) levels. Up- and down-regulated proteins/peptides indicated in *green* and *red*, respectively, had  $p < 0.01$ . *D*, same as *C* except only peptides for the indicated proteins are shown, demonstrating good agreement between the peptides used for identification and quantification of a given protein. *E*, principal component analysis of all measured peptide intensities after analysis of variance reveals groupings of technical ( $n = 2$ ) and biological replicates ( $n = 3$ ) within basal (*blue*), hypertrophy (*red*), or failure (*green*) chromatin, concomitant with excellent reproducibility of expression variation between these three groups. The axes plot peptide intensities.

these proteins reveals extensive reprogramming at the level of chromatin structure and regulation, including proteins harboring a panel of domains known to regulate transcription and to bind DNA ([supplemental Fig. 4](#)).

**Alteration in Linker to Core Histone Ratio as a Mechanism for Chromatin Remodeling**—The protein building block of chromatin is the histone molecule. The murine genome has 80 histone genes for which mass spectrometric evidence has been observed for at least 25, based on unequivocal peptide

hits, and 54, based on combinatorial induction, highlighting the complexity of functional units available for DNA packaging and genomic structure in the heart (22). In this study, disease progression is associated with isoform-specific (*i.e.* different gene products) reprogramming of histone variants (Fig. 2A). Strikingly, the ratio of linker (*i.e.* H1) to core (H2A, H2B, H3, and H4) histones was decreased during hypertrophy and returned to baseline during failure (Fig. 2B and [supplemental Fig. 3G, top panel](#)). This change in core to linker

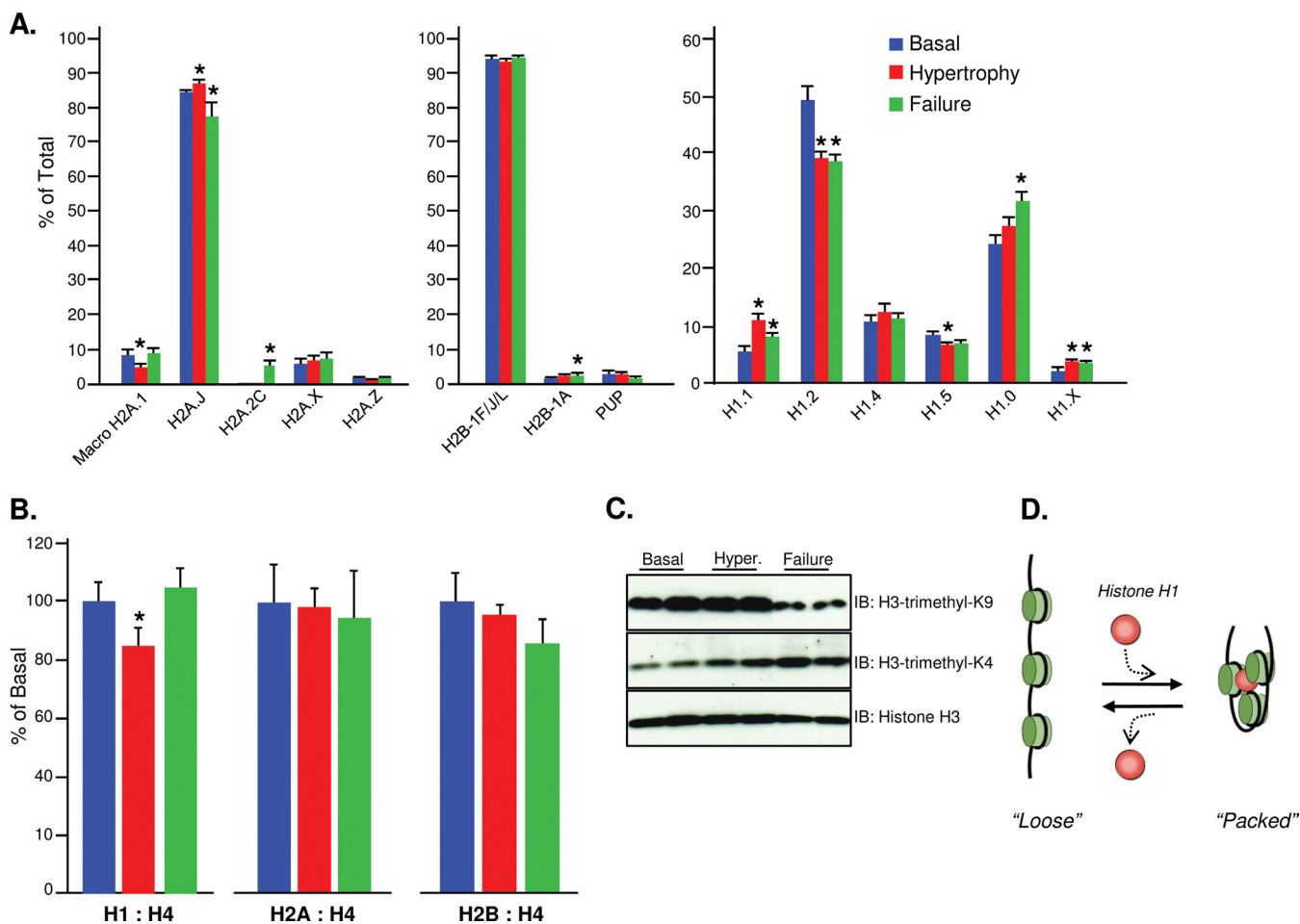


**FIG. 2. Mechanisms for genome-wide chromatin remodeling: changing the core to linker histone ratio.** *A*, global changes in gene expression with disease are associated with quantitative changes in histone families H2A, H2B, and H1 as measured by mass spectrometry. Histone H3 is absent because of extensive post-translational modification, in agreement with previous reports from other cell types (50); histone H4 has essentially only one known coding sequence. Findings were determined by spectral counting from manually validated SEQUEST results. *B*, ratio of linker (histone H1) to core (here, histone H4 is used based on the aforementioned rationale) histone variants exhibits significant global decrease during hypertrophy, returning to baseline during failure (*left panel*; data confirmed by Western blotting, see [supplemental Fig. 3G](#)). The ratio among core histones is unchanged (*middle and right panels*). *C*, the histone modifications H3K4me3 (an established activating mark (51)) and H3K9me3 (an established silencing mark (30)) were increased and decreased, respectively, serving as a readout for a global shift from hetero- to euchromatin. *D*, model for effects of alterations in core to linker histone ratio on local chromatin structure. A red circle indicates a chromatin structural protein, such as linker histone H1. “Loose” and “packed” local features would tend to favor global eu- or heterochromatin, respectively. *IB*, immunoblot.

histone ratio was associated with a global shift from hetero- to euchromatin (*i.e.* from silenced to more transcriptionally active chromatin (30, 31)), as evinced by the increase in histone mark H3K4me3 and the decrease in H3K9me3 (Fig. 2C). Although this change in linker to core histone ratio is modest (~15%; Fig. 2B), the functional impact could be profound, because it may be sufficient to affect ~15% of the coding and noncoding genome. This finding supports the concept that linker histones facilitate packaging of chromatin into higher order structures (7, 32), the local scale effects of which are represented diagrammatically in Fig. 2D.

Because these analyses are unbiased and quantitative, the opportunity exists to discover emergent properties within the data. Trend analyses reveal self-organizing modules of chro-

matin-bound proteins with similar behavior during disease progression (Fig. 3; see [supplemental Tables 1–5](#), including quantitative changes during the different disease states). Unsupervised clustering of z-score transformed data (which allows for analysis across ranges of absolute abundance) in this manner allows for determination of groups of molecules (26, 27) with nonintuitive relationships that could not be revealed by annotation and would otherwise not be examined in a traditional gain/loss of function experiment (fold changes in abundance of individual proteins are reported in the [supplemental Table 4](#)). It remains unknown at what level(s) the abundance of these proteins are principally controlled (*e.g.* transcription, nuclear translocation, degradation, and so forth).

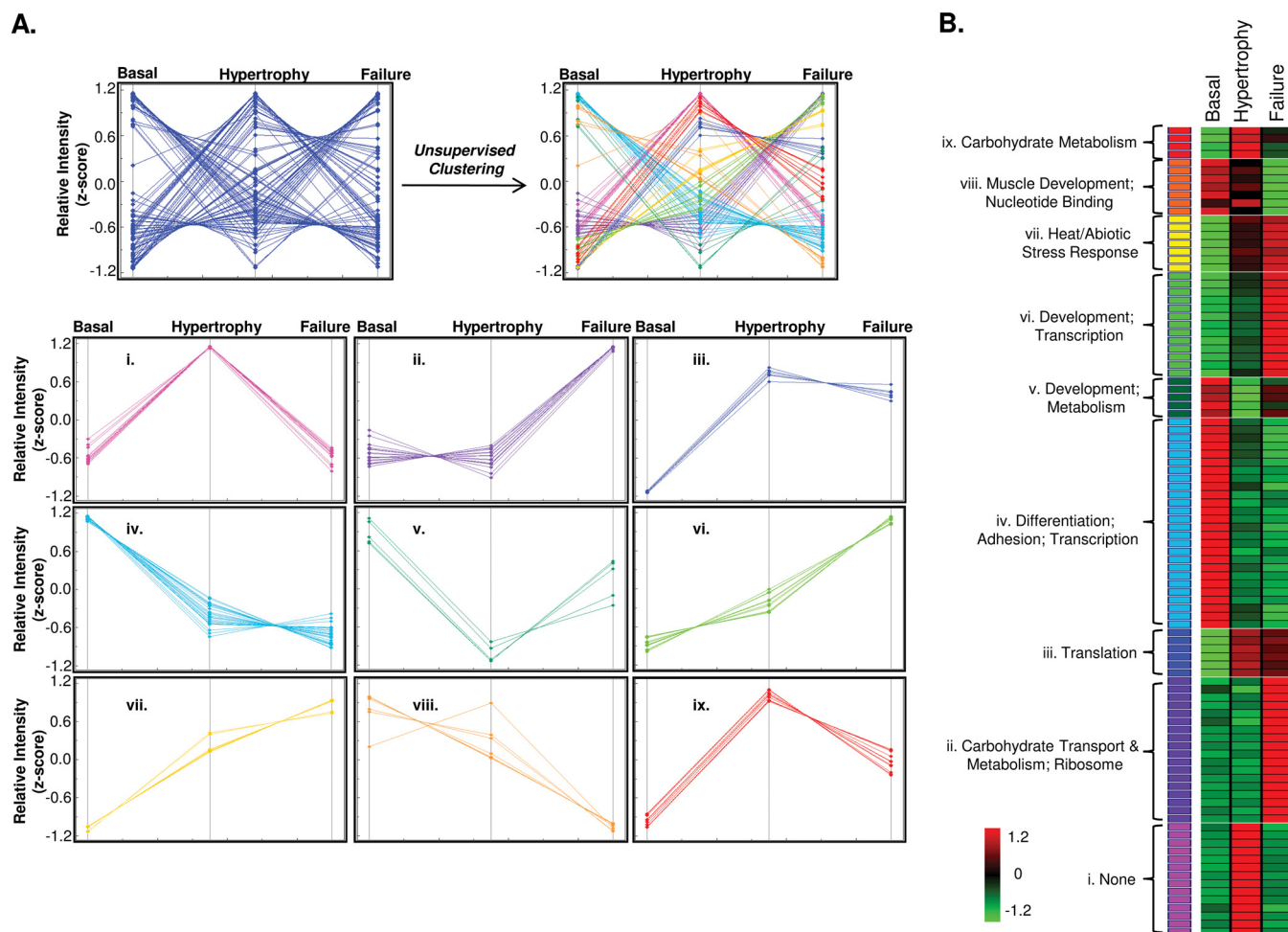


**FIG. 3. Unsupervised clustering reveals modules of chromatin regulatory proteins.** *A*, proteins with altered chromatin association during disease are displayed (*top left*; each line is an individual protein). Trend analysis produced nine clusters (*top right* and then expanded in *lower panels*) with similar behavior during disease progression (data are z-scores transformed to compare patterns of change across the entire dynamic range; see [supplemental Table 5](#) for relative quantitative information between members in a given module). *B*, heat map display of modules from *A*, indicating the Gene Ontology terms enriched in the given modules (see [supplemental Table 5](#) for list of proteins in each module). In addition to these novel features, Gene Ontology, Interpro, and Kyoto Encyclopedia of Genes and Genomes analyses revealed enrichment in various protein domains and established pathways in the cardiac chromatin data ([supplemental Fig. 4](#)).

*HMGB2 Is a Novel Regulator of Pathologic Cardiac Cell Growth*—To explore the isoform-specific roles of individual chromatin structural proteins from within modules identified in Fig. 3, small interfering RNA was used to knock down expression of two high mobility group proteins identified in our study (HMGB1 and 2) and previously implicated in chromatin structure (8, 33). Loss of HMGB2 (but not HMGB1; Fig. 4A) induced genomic structural remodeling conducive to cell growth, as measured by cell size (Fig. 4B) and some aspects of genomic reprogramming associated (20, 29) with a fetal phenotype (Fig. 4C). Although previous investigations had linked this family to cancer signaling (34, 35), this is to our knowledge the first demonstration of a functional role for HMGBs in cardiac phenotype. Microarray gene expression analyses following HMGB2 knockdown indicate that the resulting growth phenotype is the product of specific cardiac growth pathways,

including hypertrophic gene up-regulation and MAPK pathway activation, among others (Fig. 5A and [supplemental Fig. 5](#)). HMGB2 appears to be important for structural inhibition of a genome-wide growth expression program, in that genes whose expression is influenced by HMGB2 knock-down are distributed with apparent randomness across the genome (Fig. 4D). Interestingly, the role these proteins play in regulating chromatin structure is very stimulus-specific, in that hypertrophic growth induced by isoproterenol and phenylephrine induces an increase in HMGB1 and a decrease in HMGB2, whereas stimulation with endothelin-1 has the anti-thetic effect (Fig. 5B). Biochemical evidence was observed to support distinct populations of HMGB-associated chromatin, in that different amounts of each isoform were recovered depending on the use of either detergent or low pH in the chromatin isolation buffer ([supplemental Fig. 6](#)). Lastly, de-

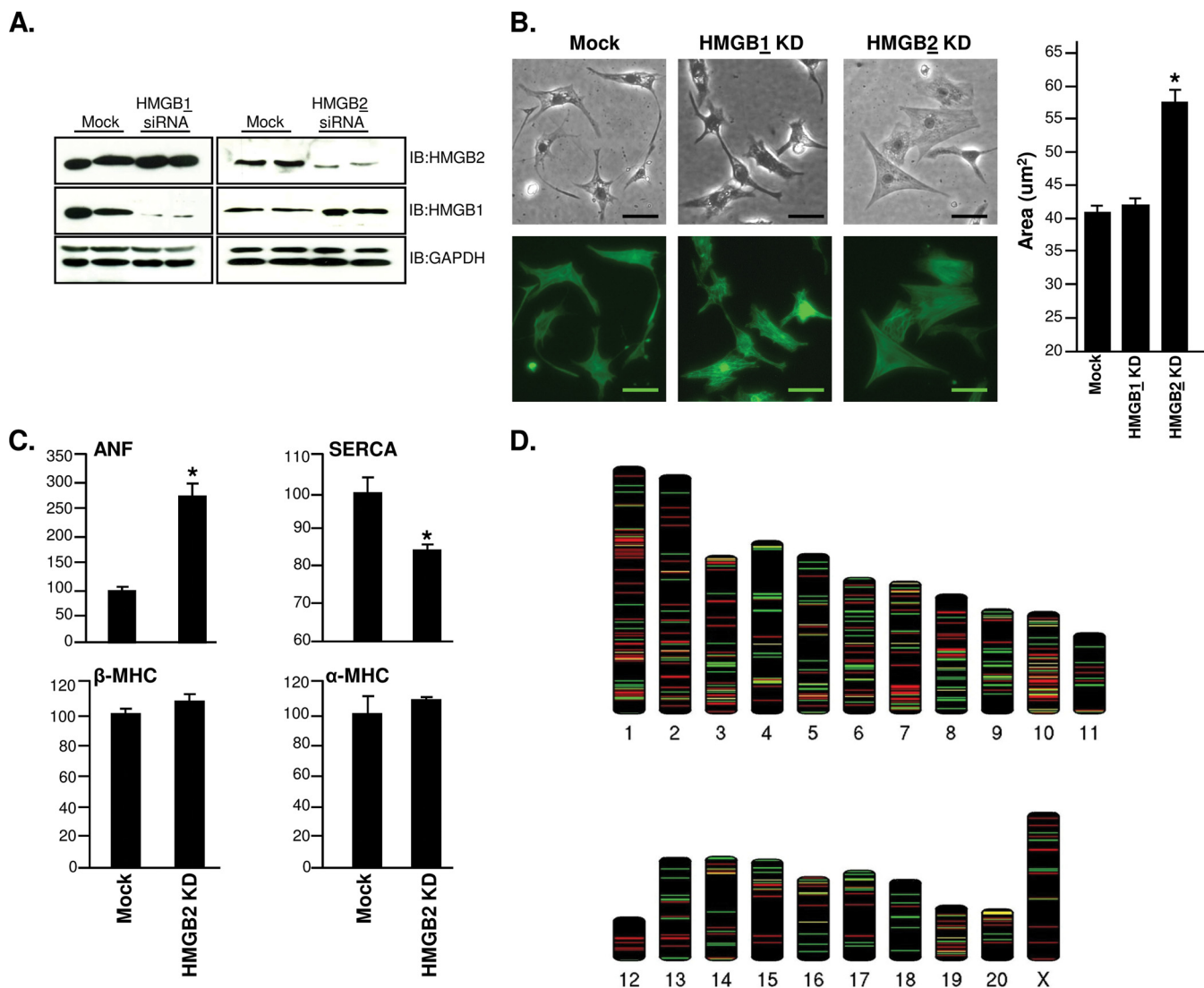


**FIG. 4. Specific chromatin structural proteins control distinct regions of the genome, enabling global changes in gene expression.** *A*, knockdown of HMGB2 leads to compensatory up-regulation of HMGB1, although the inverse does not occur. RT-PCR was also used to confirm efficacy of knockdown at mRNA level. Knockdown of HMGB2, but not HMGB1, induces neonatal cardiac myocytes to undergo hypertrophic growth akin to disease. *B*, bar indicates 50  $\mu\text{m}$ . For each condition at least 50 cells were quantified in three separate experiments, yielding 150 cells per condition. *C*, this shift in phenotype recapitulates some but not all of the gene expression changes associated with disease *in vivo* (compare *C* with [supplemental Fig. 1C](#)), suggesting that different chromatin structural proteins package distinct populations of genes. The *error bars* represent S.E. The *asterisk* indicates  $p < 0.001$ . *D*, to examine regions of the genome whose structure is maintained—and therefore transcriptional activity modulated—by HMGB2, expression microarrays were performed in the absence and presence of HMGB2 knockdown, demonstrating global effects that include all chromosomes (*yellow* indicates a bin in which some genes were up and other down-regulated; see [supplemental Table 6](#) for list of genes with altered expression following HMGB2 knockdown). *IB*, immunoblot.

creased HMGB2-dependent chromatin regulation was accompanied by a shift from hetero- to euchromatin, as shown by H3K4me3, H3K9me3, and heterochromatin binding protein-1 $\alpha$  abundance (Fig. 5C). These findings support the concept that chromatin remodeling for transcription occurs in a context-specific manner (36, 37), with different histone variants, structural proteins, and modifications specifying control of different genomic regions (38–40) (Fig. 5D).

#### DISCUSSION

Together these studies support a model in which a balance of local and global chromatin remodeling events is necessary to structurally poise all chromosomes for genome-wide changes in transcription. Evidence in support of this conjecture is the stimulus specificity of chromatin structural protein expression, the distinct localization of HMGB target genes across all chromosomes, and the alterations in HMGB protein

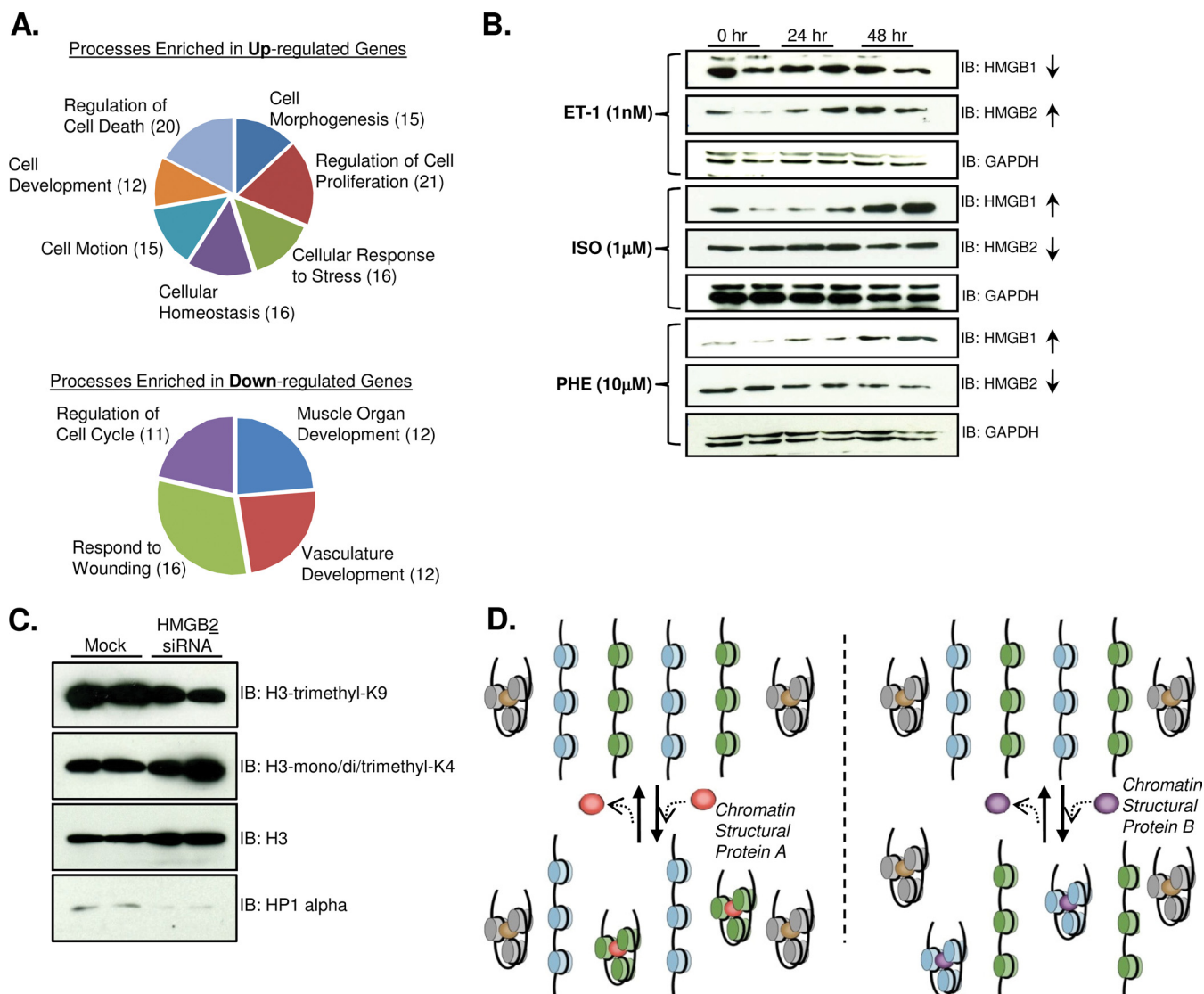


**FIG. 5. Functional impact of HMGB knockdown on gene expression and chromatin structure.** *A*, pie charts demonstrate the processes enriched in the up- or down-regulated genes detected by microarray following HMGB2 knockdown (see [supplemental Table 6](#) for list of genes with altered expression following HMGB2 knockdown). Additional bioinformatic analyses ([supplemental Fig. 5](#)) demonstrate enrichment of nucleotide-binding domains and many pathways implicated in cell growth and cardiac function/dysfunction in the genes under control of HMGB2. *B*, changes in HMGB1/2 expression at distinct times following different hypertrophic agonists in neonatal rat ventricular myocytes (these stimuli are sufficient to induce hypertrophic cell growth). *C*, HMGB2 knockdown induces a shift from hetero- to euchromatin, as documented by increased histone H3 K4 methylation, decreased K9 methylation, and increased abundance of heterochromatin binding protein 1 $\alpha$ . *D*, representation of the local chromatin remodeling events that can orchestrate global shifts in DNA accessibility. In this model, linker histones or non-histone chromatin structural proteins (like HMGs; indicated by the *red* and *purple* circles) induce specific genomic regions (indicated with the *green* or *blue* nucleosomes) to assume a more compact structure (Fig. 2D); regions not under structural regulation by the given proteins remain unaffected (*gray* nucleosomes). For simplicity, only nucleosomes and chromatin structural proteins are shown; *in vivo*, nucleosome positioning (through DNA sequence, proteins interactions, and post-translational modifications) and other position-specific chromatin modifiers likely are contributory to specifying these hypothetical populations of chromatin. This model suggests that these distinct local principles are applied globally based on different expression profiles and genomic localization of linker histones and non-histone chromatin structural proteins. *IB*, immunoblot; ET-1, endothelin-1; ISO, isoproterenol; PHE, phenylephrine.

expression and histone linker to core ratio in the setting of massive gene expression changes in disease. Decreased abundance (or knockdown, in the experimental setting) of chromatin structural proteins including linker histones and HMGs would tend to shift the equilibrium toward relaxed

chromatin (or to the *left* in Fig. 2D). This hypothesis solves the problem of how an active transcription factor “finds” the right regions of the genome to bind: commensurate with transcription factor activation, global chromatin remodeling through altered linker histone/HMG abundance (Fig. 5D) shifts the

presentation of the interphase genome to a conformation permissive for binding of transcription factors to the appropriate regions of the genome, while simultaneously masking those regions not targeted for immediate expression. Future work will be required to demonstrate whether these principles are operative in noncardiac cell types. Likewise, additional studies will be required to test the hypothesis that three-dimensional reorganization of the cardiac genome occurs reproducibly in real time, using methods (likely microscopy-based) that capture the movements of chromosomes in the anatomical context of the cell (41). It is likely that the function of chromatin structural proteins peripheral to the nucleosome is determined by local DNA sequence and chromatin-associated proteins (and their post-translational modifications) rather than being universally activating or inhibiting of transcription across the genome.

The unsupervised clustering of chromatin protein abundance provides novel insights into the global processes that control gene expression. Whether and if so, how the proteins in the modules identified in Fig. 3 are functionally connected in the cell is an exciting area of future work. Our bioinformatic analyses by gene ontology, however, yield interesting leads: modules involved in muscle development, stress response, transcription, differentiation, development, and metabolism all suggest that chromatin-bound proteins participate in various aspects of cellular homeostasis and that many of these processes are targeted in distinct ways during disease.

In addition to controlling some genes previously associated with hypertrophic growth (ANF and SERCA; Fig. 4C), our microarray studies following knockdown indicate a role for HMGB2 in the packing and regulation of other interesting cardiac-related genes (supplemental Table 6). Among genes up-regulated when HMGB2 is knocked down (suggesting that the protein normally contributes to their silencing) are Wnt5, a well studied morphogen with roles in cardiac development and disease (42), and Ras, a GTPase known to induce hypertrophic growth through sarcoplasmic reticulum disruption (43). Down-regulated genes following knockdown included HDACs, whose activity is inversely correlated with gene activation in the heart (44), supporting observations in the current study about a shift to more euchromatic phenotype in hypertrophy (Fig. 2C) or during HMGB2 knockdown (Fig. 5C), and the chromatin remodeling complex member PARP that, along with Brg1, contributes to reprogramming gene expression in hypertrophic cardiomyopathy (45). How these and many other interesting genomic candidates (supplemental Table 6) coordinately regulate the hypertrophic response to pressure overload and/or loss of HMGB2 will be interesting to explore in future work.

Chromatin remodeling is pervasive in cardiovascular development and disease (46, 47), although the mechanisms for genome-wide control of genomic structure remain unknown. Previous investigations have revealed key roles for histone-modifying enzymes in controlling transcriptional states (48),

including in the regulation of cardiac development and disease (12, 49). Other investigators have used mass spectrometry to examine chromatin-associated proteins (14, 15, 17, 18); however the present studies provide the first quantitative blueprint of chromatin binding proteins from an endogenous source combined with unbiased analysis of the changes in chromatin structural proteins during the development of disease. Our data demonstrate global shifts in the hetero- to euchromatin balance during disease progression and implicate specific roles for individual histone and other chromatin structural proteins, including HMGB2. These findings have fundamental implications for the field of chromatin biology as well as for cardiovascular and other diseases, suggesting that future therapeutic strategies may be engineered to target entire functional regions of the genome via specific chromatin structural proteins.

*Acknowledgments*—We thank Anna Paulsson, Maria Kolmakova, and Todd Kimball for technical assistance, Michael J. Zhang for contributions to early stages of this work, Michelle Parvatiyar for discussion, Robb MacLellan for isolation of NRVMs and discussion, Jeff Abramson for discussion and feedback on the manuscript, and Joe DeYoung for assistance with microarrays (all at UCLA).

S. F. and T. M. V. conceptualized the study and wrote the paper. Y. W. contributed resources and expertise. S. F. carried out all experiments except the mouse surgeries and cardiac function, which were done by S. R. and S. M.-J., and S. F., H. D. C., and T. M. V. analyzed the data.

\* This study was supported by NHLBI and NCRG grants (to T. M. V.) and the Laubisch Endowment at UCLA (to T. M. V.). Mass spectrometry instrument contract support comes from NHLBI Proteomics Contract HHSN268201000035C. The costs of publication of this article were defrayed in part by the payment of page charges. This article must therefore be hereby marked “advertisement” in accordance with 18 U.S.C. Section 1734 solely to indicate this fact.

§ This article contains supplemental material.

§ Recipient of an NHLBI, National Institutes of Health Ruth Kirschstein Post-doctoral Fellowship. To whom correspondence may be addressed: Depts. of Anesthesiology, Medicine and Physiology, David Geffen School of Medicine at UCLA, BH-557 CHS Bldg., 650 Charles Young Dr., Los Angeles, CA 90095. Tel.: 310-206-4072; E-mail: sfranklin@mednet.ucla.edu.

\*\* To whom correspondence may be addressed: Depts. of Anesthesiology, Medicine and Physiology, David Geffen School of Medicine at UCLA, BH-557 CHS Bldg., 650 Charles Young Dr., Los Angeles, CA 90095. Tel.: 310-206-4072; E-mail: tvondrisk@mednet.ucla.edu.

## REFERENCES

1. Cremer, T., and Cremer, C. (2001) Chromosome territories, nuclear architecture and gene regulation in mammalian cells. *Nat. Rev. Genet.* **2**, 292–301
2. van Steensel, B., and Dekker, J. (2010) Genomics tools for unraveling chromosome architecture. *Nat. Biotechnol.* **28**, 1089–1095
3. Luger, K., Mäder, A. W., Richmond, R. K., Sargent, D. F., and Richmond, T. J. (1997) Crystal structure of the nucleosome core particle at 2.8 Å resolution. *Nature* **389**, 251–260
4. Tremethick, D. J. (2007) Higher-order structures of chromatin: The elusive 30 nm fiber. *Cell* **128**, 651–654
5. Pruss, D., Bartholomew, B., Persinger, J., Hayes, J., Arents, G., Moudrianakis, E. N., and Wolffe, A. P. (1996) An asymmetric model for the nucleosome: A binding site for linker histones inside the DNA gyres.

- Science* **274**, 614–617
6. Graziano, V., Gerchman, S. E., Schneider, D. K., and Ramakrishnan, V. (1994) Histone H1 is located in the interior of the chromatin 30-nm filament. *Nature* **368**, 351–354
  7. Weintraub, H. (1984) Histone-H1-dependent chromatin superstructures and the suppression of gene activity. *Cell* **38**, 17–27
  8. Bustin, M. (1999) Regulation of DNA-dependent activities by the functional motifs of the high-mobility-group chromosomal proteins. *Mol. Cell. Biol.* **19**, 5237–5246
  9. Goodwin, G. H., Sanders, C., and Johns, E. W. (1973) A new group of chromatin-associated proteins with a high content of acidic and basic amino acids. *Eur. J. Biochem.* **38**, 14–19
  10. Talbert, P. B., and Henikoff, S. (2010) Histone variants: Ancient wrap artists of the epigenome. *Nat. Rev. Mol. Cell Biol.* **11**, 264–275
  11. Cairns, B. R. (2009) The logic of chromatin architecture and remodelling at promoters. *Nature* **461**, 193–198
  12. Haberland, M., Montgomery, R. L., and Olson, E. N. (2009) The many roles of histone deacetylases in development and physiology: Implications for disease and therapy. *Nat. Rev. Genet.* **10**, 32–42
  13. Ho, L., and Crabtree, G. R. (2010) Chromatin remodelling during development. *Nature* **463**, 474–484
  14. Ohta, S., Bukowski-Wills, J. C., Sanchez-Pulido, L., Alves Fde, L., Wood, L., Chen, Z. A., Platani, M., Fischer, L., Hudson, D. F., Ponting, C. P., Fukagawa, T., Earnshaw, W. C., and Rappsilber, J. (2010) The protein composition of mitotic chromosomes determined using multiclassifier combinatorial proteomics. *Cell* **142**, 810–821
  15. Zougman, A., and Wiśniewski, J. R. (2006) Beyond linker histones and high mobility group proteins: Global profiling of perchloric acid soluble proteins. *J. Proteome Res.* **5**, 925–934
  16. Gerstein, M. B., Lu, Z. J., Van, Nostrand, E. L., Cheng, C., Arshinoff, B. I., Liu, T., Yip, K. Y., Robilotto, R., Rechtsteiner, A., Ikegami, K., Alves, P., Chateigner, A., Perry, M., Morris, M., Auerbach, R. K., Feng, X., Leng, J., Vielle, A., Niu, W., Rhrissorakrai, K., Agarwal, A., Alexander, R. P., Barber, G., Brdlik, C. M., Brennan, J., Brouillet, J. J., Carr, A., Cheung, M. S., Clawson, H., Contrino, S., Dannenberg, L. O., Dernburg, A. F., Desai, A., Dick, L., Dosé, A. C., Du, J., Egelhofer, T., Ercan, S., Euskerchen, G., Ewing, B., Feingold, E. A., Gassmann, R., Good, P. J., Green, P., Gullier, F., Gutwein, M., Guyer, M. S., Habegger, L., Han, T., Henikoff, J. G., Henz, S. R., Hinrichs, A., Holster, H., Hyman, T., Iniguez, A. L., Janette, J., Jensen, M., Kato, M., Kent, W. J., Kephart, E., Khivansara, V., Khurana, E., Kim, J. K., Kolasinska-Zwierz, P., Lai, E. C., Latorre, I., Leahey, A., Lewis, S., Lloyd, P., Lochovsky, L., Lowdon, R. F., Lubling, Y., Lyne, R., MacCoss, M., Mackowiak, S. D., Mangone, M., McKay, S., Mecnas, D., Merrihew, G., Miller, D. M., 3rd, Muroyama, A., Murray, J. I., Ooi, S. L., Pham, H., Hippen, T., Preston, E. A., Rajewsky, N., Rättsch, G., Rosenbaum, H., Rozowsky, J., Rutherford, K., Ruzanov, P., Sarov, M., Sasidharan, R., Sboner, A., Scheid, P., Segal, E., Shin, H., Shou, C., Slack, F. J., Slightam, C., Smith, R., Spencer, W. C., Stinson, E. O., Taing, S., Takasaki, T., Vafeados, D., Voronina, K., Wang, G., Washington, N. L., Whittle, C. M., Wu, B., Yan, K. K., Zeller, G., Zha, Z., Zhong, M., Zhou, X., Ahringer, J., Strome, S., Gunsalus, K. C., Micklem, G., Liu, X. S., Reinke, V., Kim, S. K., Hillier, L. W., Henikoff, S., Piano, F., Snyder, M., Stein, L., Lieb, J. D., and Waterston, R. H. (2010) Integrative analysis of the *Caenorhabditis elegans* genome by the modENCODE project. *Science* **330**, 1775–1787
  17. Bartke, T., Vermeulen, M., Xhemalce, B., Robson, S. C., Mann, M., and Kouzarides, T. (2010) Nucleosome-interacting proteins regulated by DNA and histone methylation. *Cell* **143**, 470–484
  18. Chu, D. S., Liu, H., Nix, P., Wu, T. F., Ralston, E. J., Yates, J. R., 3rd, and Meyer, B. J. (2006) Sperm chromatin proteomics identifies evolutionarily conserved fertility factors. *Nature* **443**, 101–105
  19. Rockman, H. A., Ross, R. S., Harris, A. N., Knowlton, K. U., Steinhilper, M. E., Field, L. J., Ross, J., Jr., and Chien, K. R. (1991) Segregation of atrial-specific and inducible expression of an atrial natriuretic factor transgene in an in vivo murine model of cardiac hypertrophy. *Proc. Natl. Acad. Sci. U.S.A.* **88**, 8277–8281
  20. Takimoto, E., Champion, H. C., Li, M., Belardi, D., Ren, S., Rodriguez, E. R., Bedja, D., Gabrielson, K. L., Wang, Y., and Kass, D. A. (2005) Chronic inhibition of cyclic GMP phosphodiesterase 5A prevents and reverses cardiac hypertrophy. *Nat. Med.* **11**, 214–222
  21. Mitchell-Jordan, S. A., Holopainen, T., Ren, S., Wang, S., Warburton, S., Zhang, M. J., Alitalo, K., Wang, Y., and Vondriska, T. M. (2008) Loss of Bmx nonreceptor tyrosine kinase prevents pressure overload-induced cardiac hypertrophy. *Circ. Res.* **103**, 1359–1362
  22. Franklin, S., Zhang, M. J., Chen, H., Paulsson, A. K., Mitchell-Jordan, S. A., Li, Y., Ping, P., and Vondriska, T. M. (2011) Specialized compartments of cardiac nuclei exhibit distinct proteomic anatomy. *Mol. Cell. Proteomics* **10**, 703
  23. Sadygov, R. G., Cociorva, D., and Yates, J. R., 3rd (2004) Large-scale database searching using tandem mass spectra: Looking up the answer in the back of the book. *Nat. Methods* **1**, 195–202
  24. Krzywinski, M., Schein, J., Birol, I., Connors, J., Gascoyne, R., Horsman, D., Jones, S. J., and Marra, M. A. (2009) Circos: An information aesthetic for comparative genomics. *Genome Res.* **19**, 1639–1645
  25. Huang da, W., Sherman, B. T., and Lempicki, R. A. (2009) Systematic and integrative analysis of large gene lists using DAVID bioinformatics resources. *Nat. Protoc.* **4**, 44–57
  26. Kash, J. C., Tumpey, T. M., Proll, S. C., Carter, V., Perwitasari, O., Thomas, M. J., Basler, C. F., Palese, P., Taubenberger, J. K., García-Sastre, A., Swayne, D. E., and Katze, M. G. (2006) Genomic analysis of increased host immune and cell death responses induced by 1918 influenza virus. *Nature* **443**, 578–581
  27. Neubert, H., Bonnett, T. P., Rumpel, K., Hunt, B. T., Henle, E. S., and James, I. T. (2008) Label-free detection of differential protein expression by LC/MALDI mass spectrometry. *J. Proteome Res.* **7**, 2270–2279
  28. Lloyd-Jones, D., Adams, R., Carnethon, M., De Simone, G., Ferguson, T. B., Flegal, K., Ford, E., Furie, K., Go, A., Greenlund, K., Haase, N., Hailpern, S., Ho, M., Howard, V., Kissela, B., Kittner, S., Lackland, D., Lisabeth, L., Marelli, A., McDermott, M., Meigs, J., Mozaffarian, D., Nichol, G., O'Donnell, C., Roger, V., Rosamond, W., Sacco, R., Sorlie, P., Stafford, R., Steinberger, J., Thom, T., Wasserthiel-Smoller, S., Wong, N., Wylie-Rosett, J., and Hong, Y. (2009) Heart disease and stroke statistics–2009 update: A report from the American Heart Association Statistics Committee and Stroke Statistics Subcommittee. *Circulation* **119**, 480–486
  29. Rajabi, M., Kassiotis, C., Razeghi, P., and Taegtmeier, H. (2007) Return to the fetal gene program protects the stressed heart: A strong hypothesis. *Heart Fail Rev.* **12**, 331–343
  30. Bannister, A. J., Zegerman, P., Partridge, J. F., Miska, E. A., Thomas, J. O., Allshire, R. C., and Kouzarides, T. (2001) Selective recognition of methylated lysine 9 on histone H3 by the HP1 chromo domain. *Nature* **410**, 120–124
  31. Strahl, B. D., Ohba, R., Cook, R. G., and Allis, C. D. (1999) Methylation of histone H3 at lysine 4 is highly conserved and correlates with transcriptionally active nuclei in Tetrahymena. *Proc. Natl. Acad. Sci. U.S.A.* **96**, 14967–14972
  32. Thoma, F., Koller, T., and Klug, A. (1979) Involvement of histone H1 in the organization of the nucleosome and of the salt-dependent superstructures of chromatin. *J. Cell Biol.* **83**, 403–427
  33. Rattner, B. P., Yusufzai, T., and Kadonaga, J. T. (2009) HMGN proteins act in opposition to ATP-dependent chromatin remodeling factors to restrict nucleosome mobility. *Mol. Cell* **34**, 620–626
  34. Kwon, J. H., Kim, J., Park, J. Y., Hong, S. M., Park, C. W., Hong, S. J., Park, S. Y., Choi, Y. J., Do, I. G., Joh, J. W., Kim, D. S., and Choi, K. Y. Overexpression of high-mobility group box 2 is associated with tumor aggressiveness and prognosis of hepatocellular carcinoma. *Clin. Cancer Res.* **16**, 5511–5521
  35. Lee, D., Kwon, J. H., Kim, E. H., Kim, E. S., and Choi, K. Y. (2010) HMGB2 stabilizes p53 by interfering with E6/E6AP-mediated p53 degradation in human papillomavirus-positive HeLa cells. *Cancer Lett.* **292**, 125–132
  36. Fuda, N. J., Ardehali, M. B., and Lis, J. T. (2009) Defining mechanisms that regulate RNA polymerase II transcription *in vivo*. *Nature* **461**, 186–192
  37. Segal, E., and Widom, J. (2009) What controls nucleosome positions? *Trends Genet.* **25**, 335–343
  38. Schmidt, D., Wilson, M. D., Ballester, B., Schwalie, P. C., Brown, G. D., Marshall, A., Kutter, C., Watt, S., Martinez-Jimenez, C. P., Mackay, S., Talianidis, I., Flicek, P., and Odom, D. T. (2010) Five-vertebrate ChIP-seq reveals the evolutionary dynamics of transcription factor binding. *Science* **328**, 1036–1040
  39. Goldberg, A. D., Banaszynski, L. A., Noh, K. M., Lewis, P. W., Elsaesser, S. J., Stadler, S., Dewell, S., Law, M., Guo, X., Li, X., Wen, D., Chappier, A., DeKaveler, R. C., Miller, J. C., Lee, Y. L., Boydston, E. A., Holmes,

- M. C., Gregory, P. D., Grealley, J. M., Rafii, S., Yang, C., Scambler, P. J., Garrick, D., Gibbons, R. J., Higgs, D. R., Cristea, I. M., Urnov, F. D., Zheng, D., and Allis, C. D. (2010) Distinct factors control histone variant H3.3 localization at specific genomic regions. *Cell* **140**, 678–691
40. Rada-Iglesias, A., Bajpai, R., Swigut, T., Brugmann, S. A., Flynn, R. A., and Wysocka, J. (2011) A unique chromatin signature uncovers early developmental enhancers in humans. *Nature* **470**, 279–283
41. Mewborn, S. K., Puckelwartz, M. J., Abuisneineh, F., Fahrenbach, J. P., Zhang, Y., MacLeod, H., Dellefave, L., Pytel, P., Selig, S., Labno, C. M., Reddy, K., Singh, H., and McNally, E. (2010) Altered chromosomal positioning, compaction, and gene expression with a lamin A/C gene mutation. *PLoS One* **5**, e14342
42. Rao, T. P., and Kühl, M. (2010) An updated overview on Wnt signaling pathways: A prelude for more. *Circ. Res.* **106**, 1798–1806
43. Zheng, M., Dilly, K., Dos Santos Cruz, J., Li, M., Gu, Y., Ursitti, J. A., Chen, J., Ross, J., Jr., Chien, K. R., Lederer, J. W., and Wang, Y. (2004) Sarcoplasmic reticulum calcium defect in Ras-induced hypertrophic cardiomyopathy heart. *Am. J. Physiol. Heart Circ. Physiol.* **286**, H424–H433
44. McKinsey, T. A., Zhang, C. L., and Olson, E. N. (2001) Control of muscle development by dueling HATs and HDACs. *Curr. Opin. Genet. Dev.* **11**, 497–504
45. Hang, C. T., Yang, J., Han, P., Cheng, H. L., Shang, C., Ashley, E., Zhou, B., and Chang, C. P. (2010) Chromatin regulation by Brg1 underlies heart muscle development and disease. *Nature* **466**, 62–67
46. Bruneau, B. G. (2010) Chromatin remodeling in heart development. *Curr. Opin. Genet. Dev.* **20**, 505–511
47. Han, P., Hang, C. T., Yang, J., and Chang, C. P. (2011) Chromatin remodeling in cardiovascular development and physiology. *Circ. Res.* **108**, 378–396
48. Narlikar, G. J., Fan, H. Y., and Kingston, R. E. (2002) Cooperation between complexes that regulate chromatin structure and transcription. *Cell* **108**, 475–487
49. Ago, T., Liu, T., Zhai, P., Chen, W., Li, H., Molkenin, J. D., Vatner, S. F., and Sadoshima, J. (2008) A redox-dependent pathway for regulating class II HDACs and cardiac hypertrophy. *Cell* **133**, 978–993
50. Garcia, B. A., Pesavento, J. J., Mizzen, C. A., and Kelleher, N. L. (2007) Pervasive combinatorial modification of histone H3 in human cells. *Nat. Methods* **4**, 487–489
51. Nishioka, K., Chuikov, S., Sarma, K., Erdjument-Bromage, H., Allis, C. D., Tempst, P., and Reinberg, D. (2002) Set9, a novel histone H3 methyltransferase that facilitates transcription by precluding histone tail modifications required for heterochromatin formation. *Genes Dev.* **16**, 479–489